Synthesis and field emission of single-crystalline copper vanadate nanobelts

2008 Nanotechnology 19 035607

(http://iopscience.iop.org/0957-4484/19/3/035607)

Nanotechnology **19** (2008) 035607 (6pp) doi:10.1088/0957-4484/19/03/035607

Synthesis and field emission of single-crystalline copper vanadate nanobelts

Changjie Mao, Xiaojie Wang, Xingcai Wu[1], Jun-Jie Zhu[1] and Hong-Yuan Chen

School of Chemistry and Chemical Engineering, Key Lab of Analytical Chemistry for Life Science, Nanjing University, Nanjing 210093, People's Republic of China

E-mail: wuxingca@netra.nju.edu.cn and jjzhu@netra.nju.edu.cn

Received 21 September 2007, in final form 7 November 2007
Published 11 December 2007
Online at stacks.iop.org/Nano/19/035607

Abstract

Single-crystalline nanobelts of a nonstoichiometric compound $Cu_{1.55}V_2O_{6.55}$, with a thickness of 40–60 nm, width of 50–300 nm and length of several micrometers, have been synthesized on a large scale by a hydrothermal method. The structures and morphologies of the nanobelts were characterized by x-ray powder diffraction, x-ray photoelectron spectroscopy, scanning electron microscopy, transmission electron microscopy and high-resolution transmission electron microscopy. A probable growth mechanism has also been discussed. The nanobelts exhibit a turn-on field of 11.0 V μm^{-1}, which is defined as the macroscopic field required to produce a current density of 10 $\mu A\ cm^{-2}$. It is anticipated that the nanobelts can serve as a candidate material for future field emitters.

1. Introduction

In the past decade, attention has been focused on both the preparation and the properties of one-dimensional (1D) nanostructured materials, due to their distinctive geometries, novel physical and chemical properties, and potential application in nanodevices [1–5]. Some unique properties originate from the quantum-confinement effect of nanostructured materials. Thus, the study of these nanostructured materials may give new insight into the fundamental properties with the reduction of size. Metal vanadates are important functional materials, and have different properties depending on their structures and components. For example, $ReVO_4$ (Re = Pr, Er, Gd, Dy and Nd) shows catalytic performance in the oxidative dehydrogenation of propane [6], whereas silver vanadium oxide (SVO) reveals good conductivity and high lithium-insertion capability, so it has been as a cathode material in a primary lithium anode cell that SVO has made the largest impact, mainly associated with batteries for implantable medical devices [7]. Copper vanadate also exhibits good conductivity the same as SVO, and has been widely applied in lithium batteries as the anode material, and even can be used for rechargeable lithium batteries to yield specific capacity [8]. Research showed that 1D nanostructures of metals and semiconductors are helpful for electronic field emission as well as good conductance, so it is possible that 1D nanostructures of copper vanadate with good conductance also become good electronic field emitters. Recently, there are several reports about the synthesis and physical and electrochemical properties of nanosized metal vanadates [9–12]. However, to the best of our knowledge, there have been no reports on 1D nanostructure and field emission of $Cu_{1.55}V_2O_{6.55}$. Here we selected a convenient hydrothermal approach to synthesizing single-crystalline $Cu_{1.55}V_2O_{6.55}$ nanobelts, which requires neither sophisticated techniques nor catalysts, and the field emission property of the nanostructures was investigated.

2. Experimental section

The nanobelts were synthesized by a hydrothermal method. All the reagents used in the experiments were of analytical purity and were used without further purification. In a typical procedure, a mixture of 3 mmol vanadium pentoxide powder, 3 mmol cupric acetate and 3 mmol 1,6-hexanediamine was dissolved in 40 ml distilled water. This mixture was then placed into a Teflon-lined stainless-steel autoclave, sealed and

[1] Authors to whom any correspondence should be addressed.

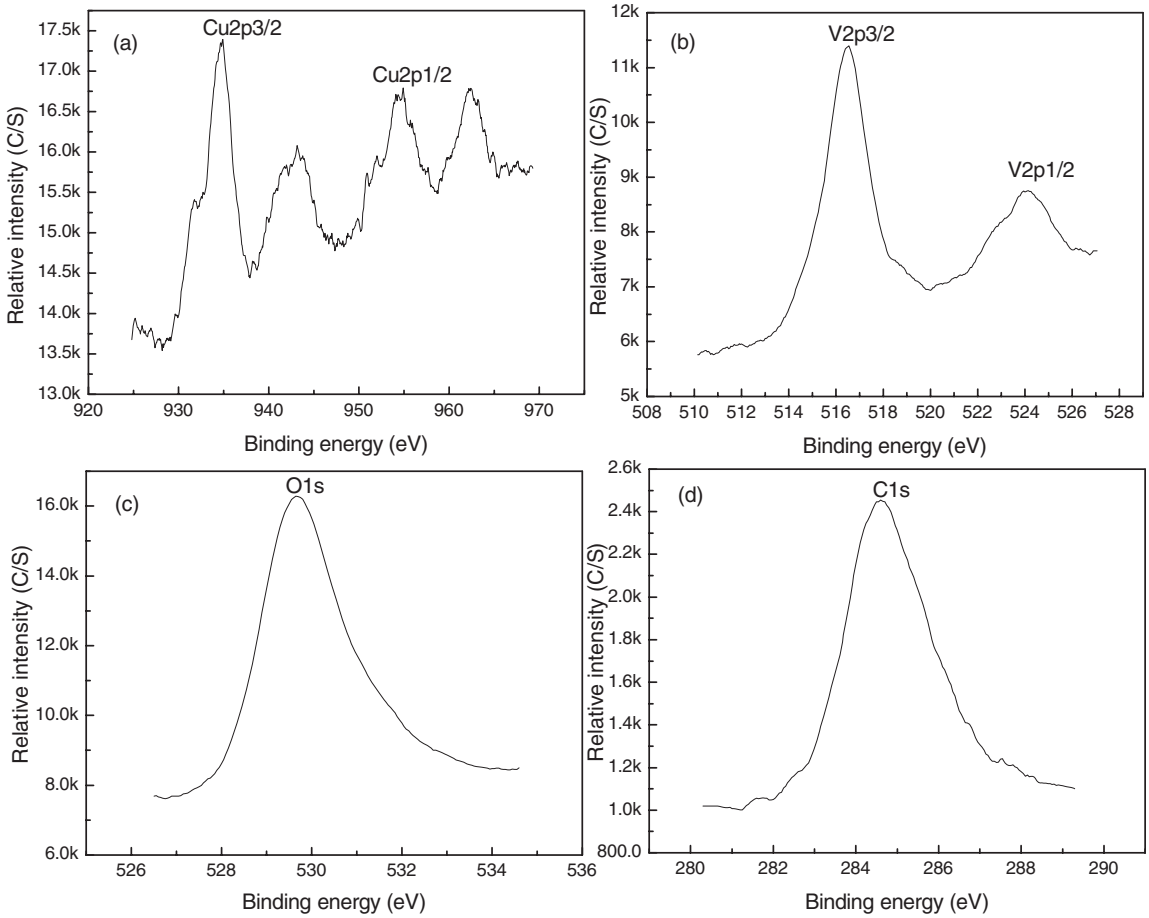

Figure 1. XPS of the as-prepared $Cu_{1.55}V_2O_{6.55}$ nanobelts: (a) Cu 2p; (b) V 2p; (c) O 1s; (d) C 1s.

maintained at 180 °C for 2 days, after which a black precipitate was formed. On cooling the sample at room temperature, the precipitate was separated by centrifuging at a rotation rate of 9000 rpm. It was then washed with distilled water and absolute ethanol in sequence, and dried in air at room temperature.

X-ray photoelectron spectra (XPS) were recorded on an ESCALAB MK II x-ray photoelectron spectrometer, using nonmonochromatized Mg Kα x-rays as the excitation source and choosing C 1s (284.6 eV) as the reference line. The chemical composition of the sample was further determined by a Plasma Quad Excell ICP-MS (TJA). The powder x-ray diffraction (XRD) pattern was determined on a Philip X'pert x-ray diffractometer with Cu Kα radiation ($\lambda = 1.5418$ Å). TEM (transmission electron microscope) images were recorded on a JEOL JEM-200CX transmission electron microscope, using an accelerating voltage of 200 kV. SEM (scanning electron microscope) images were taken by a LEO-1530VP scanning electron microscope. HRTEM (high-resolution transmission electron microscope) images were recorded on a Philips Tecanai F20 transmission electron microscope, using an accelerating voltage of 400 kV. Thermal gravity analysis (TGA) and differential thermal analysis (DTA) were performed on a Pyris 1 DSC from 30 to 700 °C at 10 °C min^{-1}. The Raman spectrum was recorded on a JY HR-800 spectrometer provided by Jobin Yvon Company at room temperature and with an excitation wavelength of 514.5 nm.

The electron field emission measurements were performed by using a parallel-plate configuration in a vacuum chamber at a pressure of 1.5×10^{-4} Pa. For the electron field emission measurement, the samples were prepared by embedding bunches of nanobelts in a silver layer. A disc of silver ink was first screen-printed on a stainless-steel substrate and the powdered $Cu_{1.55}V_2O_{6.55}$ nanobelts were distributed randomly on the surface of the silver disc. Then the samples were heated to 400 °C for 2 h in vacuum, so that the nanobelts were fixed to the thick film of silver.

3. Results and discussion

3.1. Structure and morphology

Chemical composition of the as-prepared sample was measured by ICP-MS. Copper and vanadium occupy 23.6 wt% and 24.1 wt%, respectively, so the formula of the sample was determined as $Cu_{1.55}V_2O_{6.55}$. The composition was further confirmed by XPS, as shown in figures 1(a)–(c). The values of the electron binding energy were calibrated using the C 1s peak (284.6 eV) as the internal standard. As shown in figure 1(a), the peaks at 934.8 and 954.3 eV are assigned to the electron binding energy of Cu^{2+} $2p_{3/2}$ and $2p_{1/2}$, respectively. As shown in figure 1(b), the peaks at 516.4 and 523.9 eV correspond to V^{5+} $2p_{3/2}$ and $2p_{1/2}$, respectively. As shown in

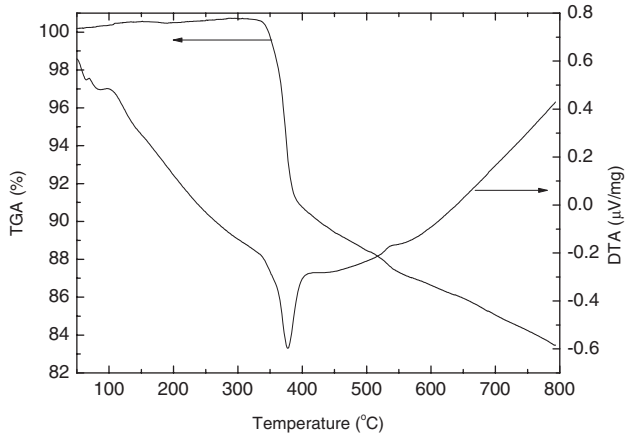

Figure 2. TGA and DTA curves of the $Cu_{1.55}V_2O_{6.55}$ nanobelts.

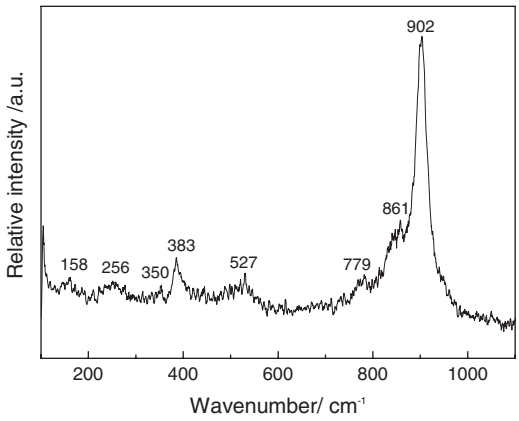

Figure 3. Raman spectrum of the $Cu_{1.55}V_2O_{6.55}$ nanobelts.

figure 1(c), the peak at 529.7 eV is assigned to the electron binding energy of O^{2-} (1s) in metal oxide. Figure 1(d) shows XPS of graphite carbon of the internal standard (C 1s, 284.6 eV). The ratio of Cu and V atoms is about 1.38:2 on the basis of the XPS composition measurement, approaching the result measured by ICP-MS.

The thermal stability of as-prepared $Cu_{1.55}V_2O_{6.55}$ nanobelts was studied by thermal gravity analysis in N_2 flowing atmosphere (including 5% oxygen). As shown in figure 2, the lost weight at 330–390 °C (9.0 wt%) corresponds to the decomposition of crystalline water while the weight loss at 390–800 °C (7.5 wt%) probably comes from the pyrolysis of residual organic templates. The entire heat treatment comprises one endothermic process as seen from the DTA curve.

To characterize the single-crystalline 1,6-hexanediamine, the Raman spectrum (figure 3) is presented in the range of 100–1100 cm^{-1}. The peaks are similar to those of copper vanadium oxides reported previously [13]. In the Raman spectrum, the bands at 902 and 527 cm^{-1} are assigned to the stretching modes of the V–O1 (the shortest) and V–O2 bonds, respectively, whereas the band at 350 cm^{-1} is assigned to the bending vibrations of the V–O1 bond. Two bands at 383 and 256 cm^{-1} are considered to originate from the bending

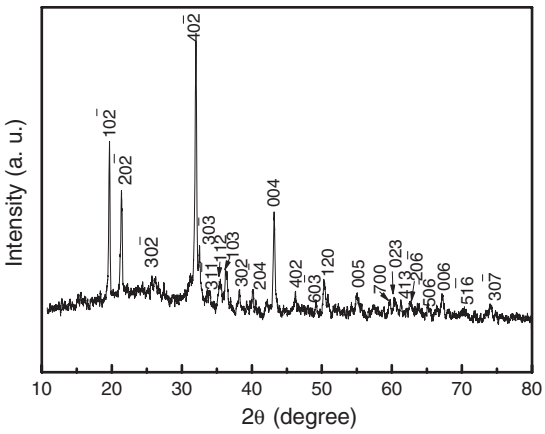

Figure 4. XRD pattern of the as-prepared $Cu_{1.55}V_2O_{6.55}$ nanobelts.

Table 1. X-ray diffraction data of $Cu_{1.55}V_2O_{6.55}$ with monoclinic cell parameters of $a = 11.68$ Å, $b = 3.678$ Å, $c = 8.974$ Å and $\beta = 111.6°$.

hkl	d_{obsd}	d_{calcd}	I/I_0
$10\bar{2}$	4.511	4.486	70
$20\bar{2}$	4.133	4.121	55
$30\bar{2}$	3.432	3.429	29
$40\bar{2}$	2.805	2.794	100
$30\bar{3}$	2.755	2.748	38
$31\bar{1}$	2.667	2.670	25
112	2.543	2.530	28
103	2.481	2.484	31
302	2.356	2.341	25
$20\bar{4}$	2.243	2.243	25
004	2.089	2.086	47
402	1.969	1.968	25
$60\bar{3}$	1.858	1.862	21
120	1.814	1.813	28
005	1.672	1.669	24
700	1.551	1.551	22
023	1.533	1.534	22
413	1.510	1.514	22
$20\bar{6}$	1.484	1.485	21
$50\bar{6}$	1.435	1.435	21
006	1.393	1.391	24
$51\bar{6}$	1.337	1.337	19
$30\bar{7}$	1.279	1.281	20

vibrations of the V–O3 and V–O2 bonds, respectively. The band at 158 cm^{-1} is assigned to external vibration of the V–O bond. The other bands are attributed to the vibrations of the Cu–O bonds.

The x-ray diffraction (XRD) pattern of the as-prepared $Cu_{1.55}V_2O_{6.55}$ nanobelts is shown in figure 4. All diffraction peaks can be perfectly indexed according to the monoclinic system with the lattice constants $a = 11.68$ Å, $b = 3.678$ Å, $c = 8.974$ Å and $\beta = 111.6°$, which approach the cell parameters of CuV_2O_5 (JCPDS card no. 43-0080: $a = 11.76$ Å, $b = 3.698$ Å, $c = 8.974$ Å and $\beta = 111.6°$). The indexed results are included in table 1.

Figures 5(a) and (b) are low-magnification SEM images of the product, which show that the product represents a belt-like morphology with width of 50–300 nm and length of

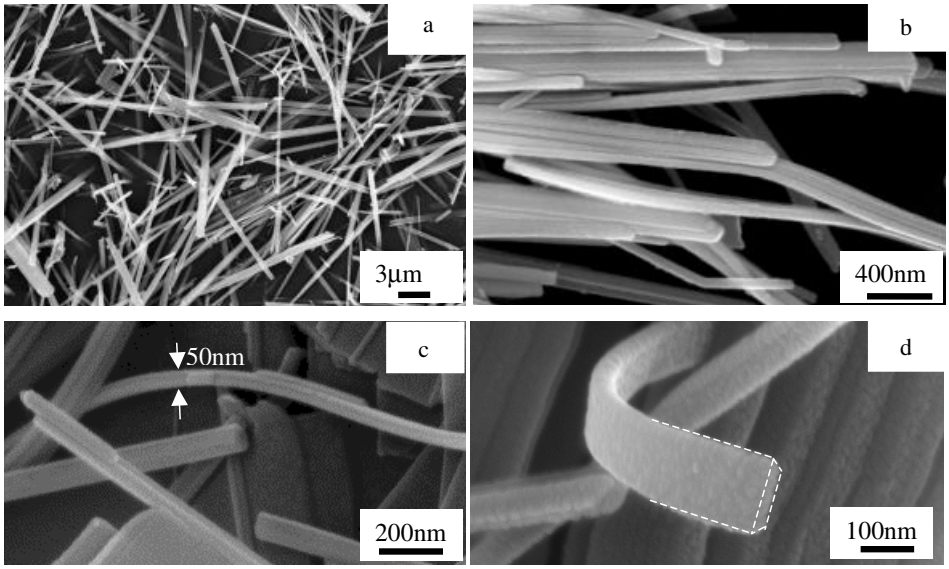

Figure 5. SEM images of the $Cu_{1.55}V_2O_{6.55}$ nanobelts: (a), (b) low-magnification images; (c), (d) high-magnification images.

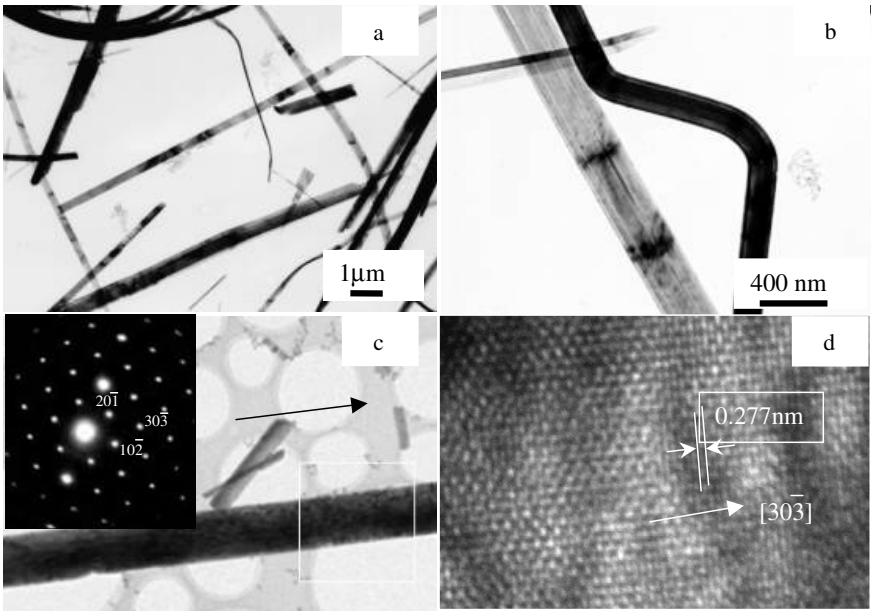

Figure 6. TEM and HRTEM images of the $Cu_{1.55}V_2O_{6.55}$ nanobelts: (a) low-magnification TEM image (JEOL); (b) high-magnification TEM image (JEOL); (c) TEM image of a single nanobelt and its SAED pattern (Philips); (d) HRTEM image of a nanobelt taken from the highlighted area (Philips).

several micrometers. Figure 5(b) still shows that they are highly flexible and can bend without breaking. To further understand the geometrical configuration of the nanobelts, the high-magnification SEM images were taken. As shown in figures 5(c) and (d), the nanobelt has the smooth side edges, a rectangular-shaped cross section on the tip surface and thickness in the range of 40–60 nm.

The TEM images shown in figure 6(a) also further reveal that the width of the $Cu_{1.55}V_2O_{6.55}$ nanobelts is in the range of 50–300 nm and that the length can reach several micrometers, and even to tens of micrometers. The characteristic variation in lateral dimension associated with a belt is clearly observed from the bending in the middle of a 1D nanostructure (figure 6(b)). Figure 6(c) reveals the morphology of an individual nanobelt, its selected-area electron diffraction (SAED) pattern is displayed in the inset and its HRTEM image is shown in figure 6(d). The clear lattice fringes exhibit good crystallinity of the product. The planar spacing is measured to be about 0.277 nm, which is in good agreement with the $(30\bar{3})$ crystalline plane of the monoclinic system of $Cu_{1.55}V_2O_{6.55}$. These lattice fringes are perpendicular to the belt axis of $Cu_{1.55}V_2O_{6.55}$ nanobelts, which demonstrates that the $Cu_{1.55}V_2O_{6.55}$ nanobelts are a single crystal with preferred growth oriented along the $[10\bar{1}]$ direction.

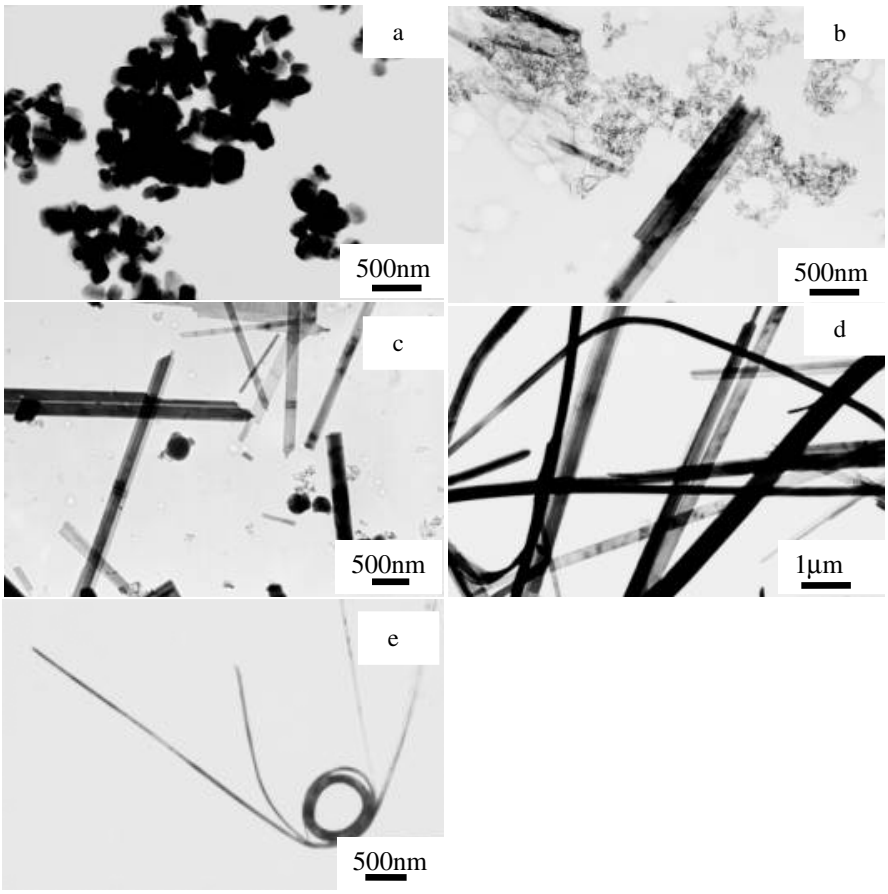

Figure 7. TEM images of the sample collected at different stages: (a) 12, (b) 24, (c) 36 and (d) 48 h. (e) A typical $Cu_{1.55}V_2O_{6.55}$ loop.

3.2. Formation mechanism

The influence of reaction conditions such as temperature, reaction time and organic template on morphology has been investigated. In contrast, without the addition of an organic template (1,6-hexanediamine), the morphology is a mixture of nanoparticles and nanobelts, and there are a large number of V_2O_5 impure phases in the product. Hence 1,6-hexanediamine plays an important role in the growth of $Cu_{1.55}V_2O_{6.55}$ nanobelts. In addition, the reaction temperature is also a key factor for the formation of $Cu_{1.55}V_2O_{6.55}$ nanobelts. When the hydrothermal temperature is lower than 60 °C, the reaction cannot happen. It may be too stable for the V_2O_5 at this temperature to be dissolved to $V_2O_6^{2-}$ to form $Cu_{1.55}V_2O_{6.55}$ (for charge equilibrium). When the reaction temperature is controlled in the range of 70–170 °C, the morphology is a mixture of nanoparticles and nanobelts. Therefore 180 °C is selected as the reaction temperature.

Time-dependent experiments were performed to gain an insight into the formation process of the sample. The nanobelts were characterized by TEM at various stages of the growth process. Figure 7 shows the TEM observation at different reaction times. As shown in figure 7(a), large particles were aggregated together in the initial reaction mixture when the reaction time reached 12 h. As the reaction time increased, the amounts of initial particles decreased. When the reaction time reached 24 h, the nanobelts began to appear (figure 7(b)), but small particles still existed. When the reaction time reached 36 h, the nanobelts became the main structure (figure 7(c)). After 48 h, initial particles were converted to $Cu_{1.55}V_2O_{6.55}$ nanobelts (figure 7(d)). We also found that there are loop-shaped nanobelts in the final product, though the yield of loops is relatively low. Figure 7(e) shows a typical $Cu_{1.55}V_2O_{6.55}$ loop with perfect circular shape, which confirms further that the as-prepared nanobelts are indeed flexible.

Therefore, the formation of $Cu_{1.55}V_2O_{6.55}$ nanobelts could be related to one proposed mechanism, the so-called 'reaction-crystallization'. It could be explained as follows: firstly, 1,6-hexanediamine combined with Cu^{2+} to form Cu (1,6-hexanediamine)$_2^{2+}$ coordinate ions; as the temperature increased, bulky vanadium pentoxide dissolved and polymerized to form $V_2O_6^{2-}$ ions under low alkali conditions. Then Cu (1,6-hexanediamine)$^{2+}$ slowly released Cu^{2+} to combine with $V_2O_6^{2-}$ ions and form $Cu_{1.55}V_2O_{6.55}$ nuclei. These nuclei aggregated gradually and formed the $Cu_{1.55}V_2O_{6.55}$ nanobelts. As reaction time increased, a large number of single-crystalline nanobelts were produced. A schematic illustration of this formation mechanism is shown in figure 8. The whole of the reaction equations are expressed as follows:

$$Cu^{2+} + 2(1,6-\text{hexanediamine}) \rightarrow Cu(1,6\text{-hexanediamine})_2^{2+} \quad (1)$$

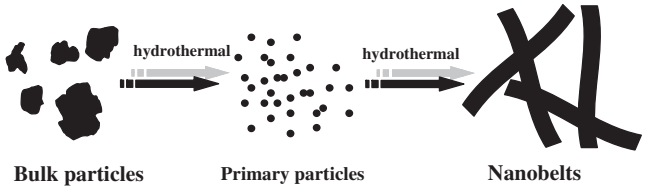

Figure 8. Schematic illustration of the growth mechanism of the $Cu_{1.55}V_2O_{6.55}$ nanobelts.

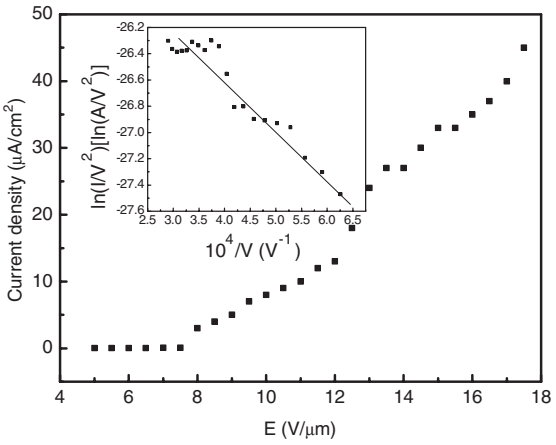

Figure 9. Field emission current applied field plot and its corresponding FN plot (inset).

$$V_2O_5 + OH^- \rightarrow V_2O_6^{2-} + H_2O \quad (2)$$

$$V_2O_6^{2-} + 1.55Cu(1,6\text{-hexanediamine})_2^{2+} \rightarrow Cu_{1.55}V_2O_{6.55} + 2 \times (1,6\text{-hexanediamine}). \quad (3)$$

3.3. Field emission measurements

To develop the new use of the $Cu_{1.55}V_2O_{6.55}$ nanobelts, the electron field emission behavior for the nanobelts was examined. The screen-printed nanobelts with cross-sectional area 1.76 cm^2 are placed into the vacuum chamber in advance. A stainless-steel probe was used as the anode to induce the electrons from the cathode nanobelts. The distance between cathode and anode was 0.2 mm. A DC voltage sweeping from 1000 to 3000 V was applied in the measurement. Figure 9 is a typical plot of the field emission current density versus the applied electric field of the $Cu_{1.55}V_2O_{6.55}$ nanobelts. The nanobelts exhibited a turn-on field of 11.0 V μm^{-1}, which is defined to be the macroscopic field required to produce a current density of 10 $\mu A\ cm^{-2}$. The maximum current obtained with our nanobelt sample is 45.0 $\mu A\ cm^{-2}$, which is lower than that of the carbon nanotube films reported recently [14], but is higher than that of NbS_2 nanowires [15]. Therefore, $Cu_{1.55}V_2O_{6.55}$ nanobelts can serve as a novel candidate for future field emitters. The inset in figure 9 shows the corresponding Fowler–Nordheim (FN) plot of the field emission property of $Cu_{1.55}V_2O_{6.55}$ nanobelts. The linearity of the FN curve indicates that the electron emission for $Cu_{1.55}V_2O_{6.55}$ nanobelts possibly results from a quantum tunneling process [16].

4. Conclusion

Monoclinic single-crystalline $Cu_{1.55}V_2O_{6.55}$ nanobelts have been synthesized by a hydrothermal method. The experiment showed that 1,6-hexanediamine promoted the formation of $Cu_{1.55}V_2O_{6.55}$ nanobelts. Through observation of the growth process, a possible growth mechanism 'reaction-crystallization' has been proposed. The field emission measurements indicate that the nanobelts have an electronic emission turn-on field of 11.0 V μm^{-1} at a current density of 10 $\mu A\ cm^{-2}$, and the maximum current density of 45.0 $\mu A\ cm^{-2}$ (at a threshold field of 18 V μm^{-1}). These findings indicate that the nanobelts have a potential future as cold cathode material, and are worthy of a further comprehensive investigation.

Acknowledgments

This work was financially supported by the National Natural Science Foundation of China (nos. 20325516, 20635020 and 90606016) and NSFC for Creative Research Group (20521503). The authors would like to thank K F Huo and Z Hu of Nanjing University for help with the field emission measurements.

References

[1] Bawendi M G, Steigerwald M L and Brus L E 1990 *Annu. Rev. Phys. Chem.* **41** 477
[2] Alivisatos A P 1996 *Science* **271** 933
[3] Weller H 1993 *Angew. Chem. Int. Edn Engl.* **32** 41
[4] Duan X, Huang Y, Cui Y, Wang J and Lieber C M 2001 *Nature* **409** 66
[5] Konvtyukhova N I and Mallouk T E 2002 *Chem. Eur. J.* **32** 435
[6] Au C T and Zhang W D 1997 *J. Chem. Soc. Faraday Trans.* **93** 1195
[7] Takeuchi K J, Marschilok A C, Davis S M, Leising R A and Takeuchi E S 2001 *Coord. Chem. Rev.* **219** 283
[8] Morcrette M, Martin P, Rozier P, Vezin H, Chevallier F, Laffont L, Poizot P and Tarascon J M 2005 *Chem. Mater.* **17** 418
[9] Yu J G, Yu J C, Ho W K, Wu L and Wang X C 2004 *J. Am. Chem. Soc.* **126** 3422
[10] Wu X C, Tao Y R, Dong L, Zhu J J and Hu Z 2005 *J. Phys. Chem.* B **109** 11544
[11] Mao C J, Wu X C, Pan H C, Zhu J J and Chen H Y 2005 *Nanotechnology* **16** 2892
[12] Zhang S Y, Li W Y, Li C S and Chen J 2006 *J. Phys. Chem.* B **111** 24855
[13] Wei Y J, Nam K W, Chen G, Ryu C W and Kim K B 2005 *Solid State Ion.* **176** 2243
[14] Milne W I, Teo K B K, Amaratunga G A J, Legagneux P, Gangloff L, Schnell J P, Semet V, ThienBinh V and Groening O 2004 *J. Mater. Chem.* **14** 933
[15] Jin Y Z, Hsu W K, Chueh Y L, Chou L J, Zhu Y Q, Brigatti K, Kroto H W and Walton D R M 2004 *Angew. Chem. Int. Edn* **43** 5670
[16] Liu B D, Bando Y, Tang C C, Xu F F and Golberg D 2005 *J. Phys. Chem.* B **109** 21521